Geomechanics and Engineering, *Vol. 23, No. 5 (2020) 493-502*
DOI: https://doi.org/10.12989/gae.2020.23.5.493

Prediction of terminal density through a two-surface plasticity model

Jongmuk Won[1a], Jongchan Kim[2b] and Junghee Park*[3]

[1]*Department of Civil and Environmental Engineering, University of Ulsan, Daehak-ro 93, Nam-gu, Ulsan 680-749, South Korea*
[2]*Department of Civil and Environmental Engineering, University of California at Berkeley, 94720-1710, CA, U.S.A.*
[3]*School of Civil, Environmental and Architectural Engineering, Korea University, 145, Anam-ro, Seongbuk-gu, Seoul 02841, South Korea*

(Received August 14, 2020, Revised November 28, 2020, Accepted November 30, 2020)

Abstract. The prediction of soil response under repetitive mechanical loadings remains challenging in geotechnical engineering applications. Modeling the cyclic soil response requires a robust model validation with an experimental dataset. This study proposes a unique method adopting linearity of model constant with the number of cycles. The model allows the prediction of the terminal density of sediments when subjected to repetitive changes in pore-fluid pressure based on the two-surface plasticity. Model simulations are analyzed in combination with an experimental dataset of sandy sediments when subjected to repetitive changes in pore fluid pressure under constant deviatoric stress conditions. The results show that the modified plastic moduli in the two-surface plasticity model appear to be critical for determining the terminal density. The methodology introduced in this study is expected to contribute to the prediction of the terminal density and the evolution of shear strain at given repetitive loading conditions.

Keywords: bounding surface; plastic modulus; pore water pressure cycle; terminal density

1. Introduction

Soils often experience many repetitive mechanical loading cycles, which lead to permanent volumetric stain accumulation. Thus, geotechnical design should consider the effect of repetitive loads on geosystems. Examples include monopile-supported wind turbines, compressed air energy storage, energy piles, and pumped hydro-storage (Peng *et al.* 2006, Anderson 2009, Pasten *et al.* 2014, Jeong *et al.* 2017, Nikitas *et al.* 2017, Moghaddas Tafreshi *et al.* 2018).

In particular, periodic fluctuations in groundwater level result in cyclic changes in effective stress despite the static loads imposed on sediments. Thereafter, pore fluid pressure oscillation can lead to sediment contraction and rebound, ground ruptures, slope instability, and even static liquefaction under drained conditions (Olson *et al.* 2000, Chu *et al.* 2003, Leroueil *et al.* 2009, Gambolati *et al.* 2015, Wu *et al.* 2018, Molina-Gomez *et al.* 2019, Sonmezer 2019).

Furthermore, cyclic changes in pore water pressure result in additional soil volume contraction followed by a decrease in normal effective stress (i.e., $\sigma'_n = K_o \cdot \sigma'_v$ - see similar cases in Boulon and Foray 1986, Suryatriyastuti *et al.* 2014). Consequently, there is a volume change-induced degradation of soil stiffness and/or skin friction between the soil-structure interface. Eventually, this degradation influences the engineering implications to the aquifer storage and recovery system using a pressure injection technique, enhanced oil recovery, and CO_2 injection and storage. Cyclic changes in pore water pressure appear to be critical in the determination of the long-term performance, safety, and serviceability of geosystems subjected to pore fluid pressure cycles, and additionally lead to the permanent accumulation of volumetric strain (Zhang *et al.* 2017); however, its prediction remains poorly understood.

We propose a unique method to anticipate the terminal void ratio e_T, which represents the permanent volumetric strain accumulation of sediments when subjected to repetitive changes in pore-fluid pressure. This study builds on earlier efforts towards modeling the soil response to repetitive loads, the bounding surface plasticity model advanced by Yu (2007), and the experimental results for a hundred of pore water pressure cycles in a triaxial cell reported by Park and Santamarina (2020). A simplified model proposed in this study estimates the terminal void ratio e_T for contractive and dilative sands when subjected to cyclic pore water pressure. We compare the terminal void ratio obtained from the modified bounding surface plasticity and the hyperbolic models to experimental results. The hyperbolic model is an empirical-based fitting equation and requires experimental results to predict the terminal void ratio. By contrast, the modified bounding surface model provides the entire repetitive load-deformation response with accumulated shear strain. In this context, the limitations of each model are discussed. This manuscript starts by outlining the underlying concepts of a bounding surface plasticity model.

2. Mathematical models

2.1 Bounding surface plasticity model

The modeling of the soil response to cyclic loading

∗Corresponding author, Research Professor
E-mail: junghee.park1905@gmail.com
[a]Assistant Professor
[b]Postdoctoral Fellow

ISSN: 2005-307X (Print), 2092-6219 (Online)

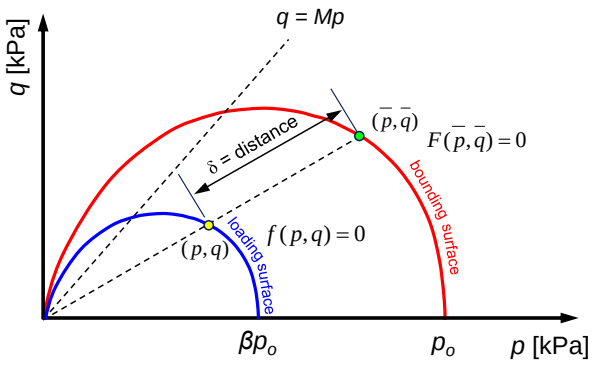

Fig. 1 Bounding surface F and loading surface f. The yellow circle indicates the current stress state (p, q) on the loading surface f and the green circle denotes the image point on the bounding surface F. The β-value corresponds to the distance $\delta = 0$ as $\beta \rightarrow 1$ while $\delta = \delta_{max}$ when $\beta \rightarrow 0$ (Yu 2007)

leads to the development of bounding surface plasticity (Dafalias and Popov 1975, Krieg 1975, Manzari and Dafalias 1997, Yu 2007, Hu *et al.* 2012, Pisanò and Jeremić 2014). The bounding surface plasticity model includes two surfaces: a loading surface f and a bounding surface F. This two-surface plasticity model does not require the tracking of the yield surface evolution (i.e., size and location) to compute the plastic strain increment but considers a continuous yield inside the bounding surface. The plastic modulus H determines the permanent volumetric or shear strain accumulations and, this modulus is a function of the distance δ between the current stress state and the image point on the bounding surface. This model allows a smoother transition from elastic to plastic states in comparison to multi-surface plasticity. This smooth transition provides an effective description of the cyclic behavior of sand and clay (Yu *et al.* 2007).

2.1.1 Loading

This study uses the mean effective stress $p' = (\sigma'_1+\sigma'_3)/2$ and the deviatoric stress $q = (\sigma'_1-\sigma'_3)/2$ where σ'_1 and σ'_3 are the effective axial stress and confining stress. Then, the current stress state (p, q) defines the loading surface f and the corresponding image point $(\bar{p},\bar{q})$ describes the bounding surface F in the context of plastic volumetric strain ε^p_p as follows (Fig. 1):

$$f(p,q,\varepsilon_p^p)=\left(\frac{q}{Mp}\right)^n+\frac{1}{\ln r}\ln\left(\frac{p}{\beta\cdot p_o}\right)=0 \tag{1}$$

$$F(\bar{p},\bar{q},\varepsilon_p^p)=\left(\frac{\bar{q}}{M\bar{p}}\right)^n+\frac{1}{\ln r}\ln\left(\frac{\bar{p}}{p_o}\right)=0 \tag{2}$$

where M is the critical stress friction angle, r is the spacing ratio, n is the material constant, and p_o is the preconsolidation pressure. The β-value is an indicator of the distance δ between the current state of stress (p, q) and its image point $(\bar{p},\bar{q})$ and is in the range of $0 < \beta < 1$. Note that the bounding surface F corresponds to the Cam-Clay model as the material constant $n \rightarrow 1$ and the spacing ratio $r \rightarrow 2.718$ (Eq. (2), Yu *et al.* (2007)).

The total volumetric ε^p and deviatoric ε^q strains caused by a successful consecutive loading and unloading cycle consist of elastic and plastic parts. First, the bulk modulus B and shear modulus G allow us to calculate the elastic volumetric $\varepsilon^p{}_e$ and deviatoric $\varepsilon^q{}_e$ strains, and associated parameters include the void ratio e, recompression index κ, and Poisson's ratio of the soil matrix ν:

$$B=\frac{p'(1+e)}{\kappa} \tag{3}$$

$$G=\frac{3p'(1+e)(1-2\nu)}{2\kappa(1+\nu)} \tag{4}$$

Then, the plastic modulus H_{load} during the loading stage is a function of the plastic modulus H_b calculated at the image point $(\bar{p},\bar{q})$ on the bounding surface F, a model constant H_R associated with reloading, and the accumulated plastic shear strain ε_q^p with a model constant k:

$$H_{load}=H_b+H_R\times\left(\frac{1-\beta}{\beta}\right)\times(1+\varepsilon_q^p)^k \tag{5}$$

This plastic modulus H_{load} estimates the plastic volumetric $\varepsilon^p{}_p$ and deviatoric strain $\varepsilon^q{}_p$ at the current stress state. The bounding surface F should satisfy that loading from a plastically-deforming state will lead to another plastically deforming state (i.e.,, the consistency condition). Thereafter, the chain rule and Rowe's stress-dilatancy relation lead to the final form of the plastic modulus H_b at the image point $(\bar{p},\bar{q})$ (see details in Yu 2007 and the derivation in Park 2018):

$$H_b=\frac{n(m-1)(1+e_o)}{(\lambda-\kappa)\bar{p}\ln r}\left[1-\frac{m\cdot\left(\frac{\bar{q}}{M\bar{p}}\right)^n}{1+(m-1)\left(\frac{\bar{q}}{M\bar{p}}\right)^n}\right] \tag{6}$$

where λ is the compression index. The m is a material constant associated with the critical state friction angle M, compression λ and recompression κ indexes and the material constant n (Eq. (1)):

$$m=\frac{2}{3}\frac{[M(6-M)]^n-(3M)^n}{\Lambda(6-M)(3M)^{n-1}} \tag{7}$$

where Λ corresponds to $(\lambda-\kappa)/\lambda$. There remains one unknown value to compute the plastic modulus H_b at the image point $(\bar{p},\bar{q})$ which is the mean effective stress $\bar{p}$; then, a rearrangement of Eq. (2) leads to the computation for the mean effective stress $\bar{p}^{(1)}$ that corresponds to $H_b{}^{(1)}$ (Fig. 2):

$$\bar{p}^{(1)}=p_o\exp\left[-\left(\frac{q_1}{Mp_1}\right)^n\ln r\right] \quad \text{where } p_0=p^*\exp\left[\left(\frac{q^*}{Mp^*}\right)^n\ln r\right] \tag{8}$$

Note that p^* and q^* are crossover points between the

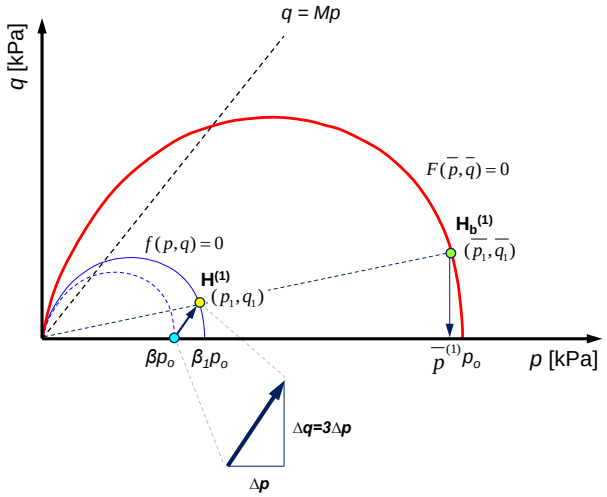

Fig. 2 Loading surface f after one stress increment Δp. $H^{(1)}$ denotes the plastic modulus on the current loading surface f (solid blue line) and $H_b{}^{(1)}$ indicates the plastic modulus on the bounding surface F (red line). Note: the superscript $^{(1)}$ denotes the first stress increment. The yellow circle indicates the current state of stress and the green circle indicates the image point on the bounding surface

critical state line and the 1:3 slope line from the end of the preconsolidation stage in the p-q diagram.

Again, the β-parameter is an indicator to represent the distance δ (Fig. 1). Thus, the plastic modulus H_{load} reaches H_b as $\beta \rightarrow 1$; in contrast, H_{load} tends to be infinite ∞ when $\beta \rightarrow 0$ [Eq. (5) and Fig. 1]. The computation of the β-value at the current stress state (p_1, q_1) follows (Fig. 2 and Eq. (1)):

$$\beta_1 = \frac{p_1}{p_o \exp\left[-\left(\frac{q_1}{Mp_1}\right)^n \ln r\right]} \tag{9}$$

Finally, we can obtain the plastic modulus H_{load} at the current stress state during the loading stage (Eqs. (5), (6), and (9)).

Bounding surface plasticity assumes that a stress increment (Δp, Δq) to the current stress state results in the same plastic volumetric strain increment at both the loading f and bounding F surfaces (Dafalias and Herrmann 1982, Bardet 1986). The plastic potential g used in this study adopts the non-associated flow rule (i.e., $f \neq g$):

$$g(p,q) = m \ln\left[1 + (m-1)\left(\frac{q}{Mp}\right)^n\right] + n(m-1)\ln\frac{p}{C} \tag{10}$$

The constant C determines the size of the plastic potential surface and $g(p, q) = 0$ returns the constant C. Then, the increment of the plastic volumetric $\Delta\varepsilon^p{}_p$ at the current stress state (p_1, q_1) is:

$$\Delta\varepsilon_p^p = \frac{1}{H_{load}}\left(\frac{\partial f}{\partial p}\Delta p + \frac{\partial f}{\partial q}\Delta q\right)\frac{\partial g}{\partial p} = \frac{1}{H_b}\left(\frac{\partial F}{\partial \bar{p}}\Delta\bar{p} + \frac{\partial F}{\partial \bar{q}}\Delta\bar{q}\right)\frac{\partial g}{\partial \bar{p}} \tag{11}$$

Three associated terms in Eq. (11) can be expressed as:

$$\frac{\partial f}{\partial p} = -\frac{n\cdot\left(\frac{q}{Mp}\right)^n}{p} + \frac{1}{p\ln r} \tag{12}$$

$$\frac{\partial f}{\partial q} = -\frac{n\cdot\left(\frac{q}{Mp}\right)^n}{q} \tag{13}$$

$$\frac{\partial g}{\partial p} = -\frac{(m-1)mn\cdot\left(\frac{q}{Mp}\right)^n}{\left[(m-1)\left(\frac{q}{Mp}\right)^n + 1\right]} + \frac{(m-1)n}{p} \tag{14}$$

Then, normality and co-axiality enable computing the deviatoric $\Delta\varepsilon^p{}_q$ strains:

$$\Delta\varepsilon_q^p = \Delta\varepsilon_p^p \frac{m\left(\frac{q}{p}\right)^{n-1}}{M^n - \left(\frac{q}{p}\right)^n} \tag{15}$$

Bulk modulus B and shear modulus G provide the calculation of the elastic volumetric strain ($\varepsilon^p{}_e$) and deviatoric strain ($\varepsilon^q{}_e$) for stress increment Δp and Δq:

$$\Delta\varepsilon_p^e = \frac{\Delta p}{B} \tag{16}$$

$$\Delta\varepsilon_q^e = \frac{\Delta q}{3G} \tag{17}$$

2.1.2 Unloading

The plastic modulus for unloading H_{unload} is also a function of the β-parameter:

$$H_{unload} = H_u \times \left(\frac{1}{1-\beta}\right) \tag{18}$$

where H_u is the model constant associated with the unloading hardening. The replacement of H_{load} into H_{unload} in Eq. (11) leads to the computation of $\Delta\varepsilon^p{}_p$ during unloading followed by $\Delta\varepsilon^p{}_q$, $\Delta\varepsilon^p{}_e$, and $\Delta\varepsilon^q{}_e$ (note: Δp and Δq at the unloading stage have negative values and denote the stress decrement at the unloading stage). The total volumetric strain is $\varepsilon_p = \Delta\varepsilon^p{}_p + \Delta\varepsilon^p{}_e$ and is used to estimate the evolution of the void ratio e as follows:

$$e_{i+1} = e_0 - \varepsilon_p(1+e_0) \tag{19}$$

where the subscript i indicates the void ratio for two consecutive loading steps. The key equations for the two-surface plasticity model addressed above enable establishing the load-deformation response of soil in the p'-q-e-ε_q space at a given repetitive loading condition.

2.2 Hyperbolic model

A substantial decrease in the void ratio of soil (e.g.,

contraction or dilation) under repetitive loading occurs in the first few cycles and the rate of change decreases as the number of loading cycles i increases. This observation implies that the void ratio evolves towards a stable deformation state known as the terminal void ratio e_T as the number of cycles approaches infinity. This study adopts a modified accumulation model to estimate the terminal void ratio e_T for the given dataset (Park and Santamarina 2019):

$$e_i = e_T + (e_0 - e_T)\left[1+\left(\frac{i}{N^*}\right)^{\eta}\right]^{-1} \quad (20)$$

where η is a fitting parameter that varies from 0-to-1 and i indicates the number of loading cycles. The void ratio e_i is the void ratio measured after the i^{th} cycle. The initial void ratio e_o corresponds to $i = 0$, and the terminal void ratio e_T is the asymptotic void ratio as $i \to \infty$. Finally, the model parameter N^* is the number of cycles required for a given soil to compact to half of the asymptotic contraction, that is, $(e_o - e_T)/2$.

The modified hyperbolic model fitted to the experimental results provides the terminal void ratio e_T as well as N^*. Moreover, the modified accumulation model can adequately capture the evolution of the void ratio with increasing number of cycles i since the alternation of three unknown parameters namely e_T, N^*, and η describes an extensive range of the dataset. Additionally, the hyperbolic model is relatively simple to use for estimating the terminal void ratio compared to the two-surface plasticity model. However, the hyperbolic model does not provide the evolution of either the void ratio or the shear/volumetric strain during loading and unloading. To compare the hyperbolic model with the two-surface plasticity model, this study estimates the terminal void ratio e_T using both models for a specimen subjected to repetitive changes in pore water pressure.

3. Prediction of terminal void ratio

3.1 Experimental data

This section reports the estimation of the terminal void ratio e_T using the modified two-surface plasticity model for a recently published dataset of Park and Santamarina (2020). They prepared saturated KAUST 20/30 sand specimens in a triaxial cell and monitored volume change during the repetitive change in pore water pressure. Table 1 summarizes the KAUST 20/30 sand properties that include particle diameter d, roundness R, coefficient of uniformity C_u, maximum e_{max} and maximum e_{min} void ratio, and friction angle at constant volume shear ϕ_{cs} [note: This study uses the critical state parameter $M = 1.2436$ for all cases calculated from ϕ_{cs} where $M = 6\sin\phi_{cs}/(3\text{-}\sin\phi_{cs})$].

They tested fourteen sand specimens: seven cases for contractive and seven cases for dilative side. Table 2 summarizes the experimental conditions: initial void ratio e_o, initial mean effective stress p'_o, constant deviatoric stress q, mean effective stress at the end of the pressurization cycle p'_{min} and at the end of the depressurization cycle p'_{max},

Table 1 Properties of KAUST 20/30 sand

Property	d [mm]	R	C_u	e_{max}	e_{min}	ϕ_{cs}
	0.60 ~ 0.85	0.6	1.2	0.786	0.533	31°

Table 2 Test conditions (after Park and Santamarina 2020)

	Test No.	e_o	p'_o [kPa]	q [kPa]	p'_{min} [kPa]	p'_{max} [kPa]	Δu_w [kPa]
Contractive	1	0.7065	2806.6	50	150	250	100
	2	0.7027	2806.6	50	140	250	110
	3	0.7031	2806.6	50	125	250	125
	4	0.6828	2806.6	50	110	250	140
	5	0.6722	2806.6	50	100	250	150
	6	0.6660	4210.0	75	150	375	225
	7	0.6783	1403.3	25	50	125	75
Dilative	8	0.5900	2806.6	50	195	250	55
	9	0.6021	2806.6	50	165	250	85
	10	0.6015	2806.6	50	125	250	125
	11	0.6025	2806.6	50	110	250	140
	12	0.6000	2806.6	50	97	250	153
	13	0.5965	2806.6	50	95	250	155
	14	0.6032	2806.6	50	90	250	160

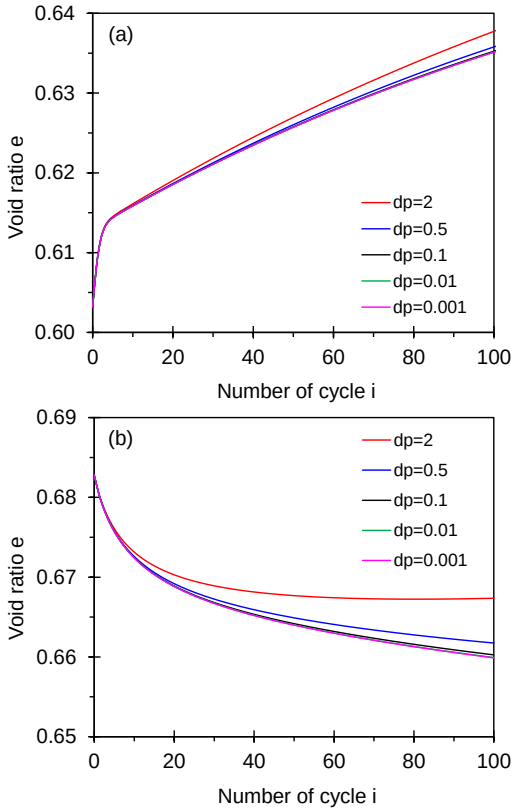

Fig. 3 Effect of step size - Void ratio e versus the number of cycles i with different stress increment Δp for dilative and contractive cases. (a) Dilative - No. 14 and (b) Contractive - No. 4 (Table 2)

and cyclic pressure amplitude Δu_w. The total number of pore

fluid pressure cycles is 100 for all cases, and the depressurization corresponds to loading while pressurization is unloading (Details in Park and Santamarina (2020)).

3.2 Numerical implementation - Bounding surface plasticity model

This study computed the total volumetric strain ε_p and void ratio e for each loading and unloading step (Δp, Δq) using Eqs. (11), (15), and (19) (note: the deviatoric stress q is constant; thus, $\Delta q = 0$ in this work). Fig. 3 plots the void ratio versus the number of cycles for different stress increment Δp. The results show that the variation of the void ratio e becomes almost negligible when $|\Delta p| < 0.01$ kPa. Therefore, the stress increment Δp selected for numerical implementation in this study was 0.01 kPa for loading steps and -0.01 kPa for unloading steps. The selection of $\Delta p = 0.01$ kPa showed a comparable result with $\Delta p = 0.001$ kPa (Fig. 3).

This study used the trust-region algorithm to obtain the best-modeled void ratio profile for the given observational data. The step for each optimized parameter and function tolerance (difference of e values) for the stopping criteria was 10^{-6} and the least-squares sense was used to evaluate the best-modeled void ratio profile. The material-dependent parameters such as n, r, λ, and κ (in Eqs. (1), (3), and (6)) were consistent throughout this study since the experimental dataset originates from KAUST 20/30 sand. Therefore, we evaluated the seven model parameters such as H_u, H_R, n, k, λ, κ, and r based on test No. 7 first (Table 2). Thereafter, we used the four-model parameters n, k, λ, and κ obtained from test No. 7 in the optimization analysis for the rest of the cases to evaluate best-fitted H_u, H_R, and r. Table 3 summarizes the upper and lower bounds for the seven parameters. These values are consistent with a previous investigation of the stress-strain response of sand under repetitive loading conditions (Yu 1998, Yu and Khong 2003, Yu *et al.* 2007).

3.3 Modification - Model constant H_u

The two-surface plasticity model introduced in the previous section has the following limitation: As the number of cycles i increases, (1) the plastic modulus for loading H_{load} reaches an asymptotic value (Eq. (5)) while the plastic modulus for unloading H_{unload} is constant (Eq. (18)) as illustrated in Fig. 4(a). Thus, there is a constant difference between the plastic moduli for loading and unloading appears. From the physical point of view, this analysis implies that plastic strain accumulation will occur until the number of cycles i reaches infinity (Fig. 4(b)). The existing model leads to a continuous decrease or increase in void ratio at $i \rightarrow \infty$; however, this is not consistent with the long-term response of sands (i.e., there exists a terminal void ratio).

The observation addressed above indicates that the existing model is not appropriate for predicting the terminal void ratio and thus requires modification. A previous study introduced an intergranular strain concept to a hypoplastic constitutive model to overcome the unceasing decrease or

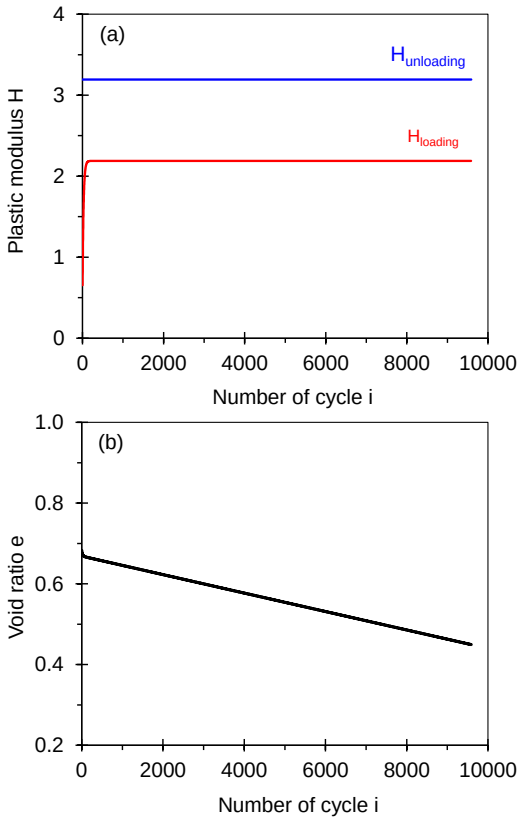

Fig. 4 Two-surface plasticity model. (a) Plastic modulus H computed by using the existing model versus number of cycles i during loading H_{load} and unloading H_{unload} and (b) Evolution of void ratio estimated from the existing model versus number of cycle i

Table 3 Upper and lower bounds of parameters and optimized values for test No. 7

Parameter	H_u	H_R	n	k	λ	κ	r	R^2
Upper bound	5	5	5	1000	0.025	0.008	19.2	-
Lower bound	0.01	0.01	1	100	0.0135	0.005	5	-
Optimized values for test No. 7	0.096	0.005	2.173	236.56	0.0147	0.0077	8.216	0.9888

increase in void ratio as the number of cycles reaches infinity (Niemunis and Herle 1997). Here, we assumed that the model constant H_u (Eq. (21)) linearly increases as the number of cycles i increases:

$$H_u = \left[\alpha \times (i-1) + 1\right] H_{uo} \quad (\alpha > 0) \tag{21}$$

where α is the slope of the model constant H_u and H_{uo} is the initial value of H_u. Fig. 5(a) shows the plastic moduli for loading H_{load} and unloading H_{unload} versus number of cycle i computed from the modification (Eq. (21)). The plastic moduli H_{load} and H_{unload} linearly increase and the gap between two plastic moduli becomes significant as the number of cycles i increases. The plastic volumetric strain at the loading and unloading stage now decreases with the number of cycles, and consequently, the void ratio appears to reach an asymptotic value (Fig. 5(b)).

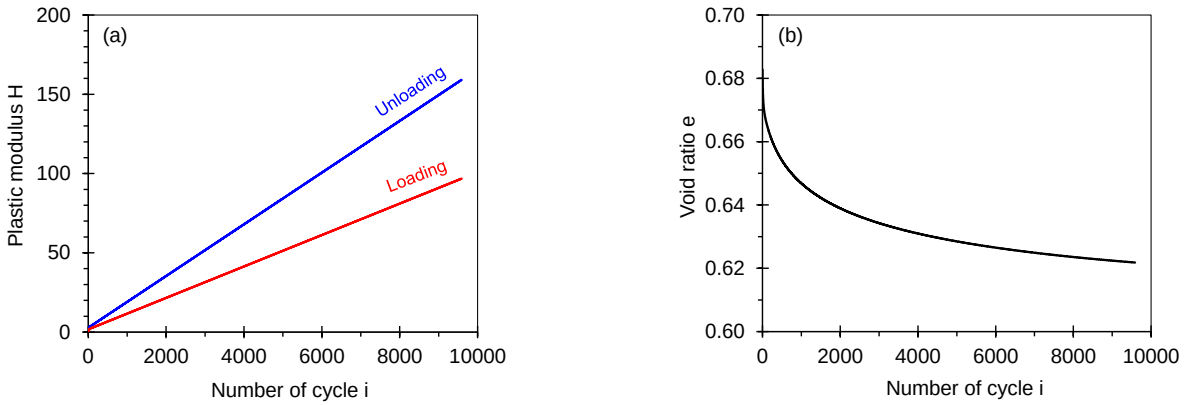

Fig. 5 Model modification. (a) Plastic modulus H computed after modification versus number of cycle i during loading H_{load} and unloading H_{unload} and (b) Evolution of void ratio estimated from the modification versus number of cycle i

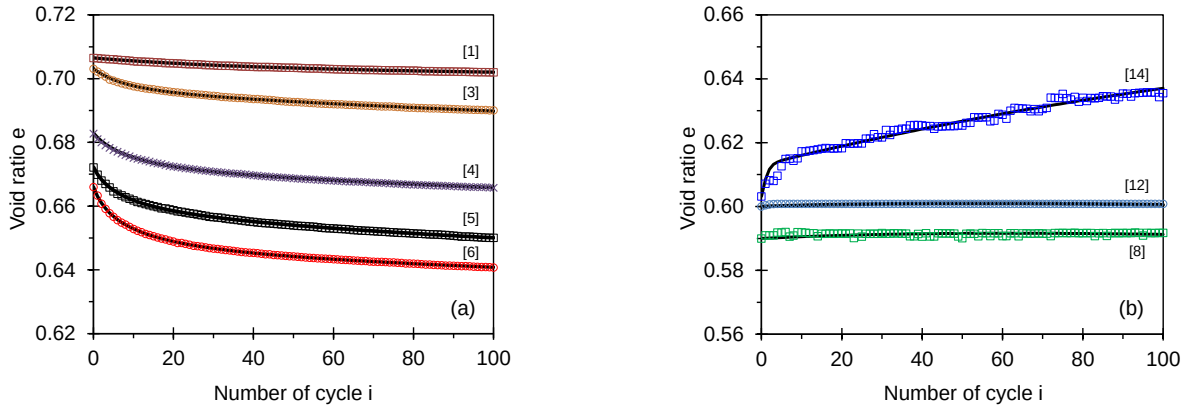

Fig. 6 Evolution of void ratio as a function of number of cycle i. (a) Contractive cases and (b) Dilative cases. Symbols indicate the experimental results from Park and Santamarina (2020) and lines indicate the modified two-surface plasticity model used in this study. Numbers in brackets [#] indicate the case No. in Table 4

Table 4 Optimized parameters for the two-surface plasticity model and the terminal void ratio estimated using this model

	Test No.	H_u	H_R	k	$\alpha \times 10^3$	R^2	e_T	N_T
Contractive	1	2.852	0.176	903.670	0.696	0.999	0.6526	16393
	2	2.800	0.179	764.240	0.105	0.733	0.5330 (e_{min})	39005
	3	1.154	0.046	855.646	3.432	0.998	0.6092	17153
	4	2.634	0.048	999.997	5.883	0.999	0.6221	9392
	5	2.695	0.031	988.454	14.705	1.000	0.6135	7146
	6	2.463	0.016	912.790	5.559	1.000	0.5952	10098
	7	4.229	0.132	692.163	1.888	1.000	0.5607	17605
Dilative	8	1.464	0.200	649.546	4.307	-0.836	0.5916	62
	9	1.817	0.192	597.652	1.054	0.292	0.6033	65
	10	1.963	0.189	564.740	0.052	-0.702	0.6031	51
	11	2.133	0.188	526.152	0.082	-95.330	0.6035	34
	12	2.988	0.243	260.893	0.041	-5.392	0.6010	54
	13	1.796	0.239	373.958	0.075	0.546	0.6047	65
	14	0.166	0.083	998.93	1.511	0.972	0.6513	338

Note: In all cases, $n = 2.173$, $\lambda = 0.0147$, $\kappa = 0.0077$, N_T: number of cycles required for e_T

3.4 Estimation of terminal void ratio

This section reports detailed results for the estimation of the terminal void ratio using the bounding surface plasticity model. The determination of the terminal void ratio consists of four stages:

Table 5 Optimized parameters for the hyperbolic model and the terminal void ratio estimated using this model

	Case No.	e_T	N^*	η	R^2
Contractive	1	0.628	8,215	0.629	0.9933
	2	0.667	10,709	0.449	0.8389
	3	0.598	9,275	0.425	0.9940
	4	0.571	7,417	0.391	0.9889
	5	0.542	6,175	0.379	0.9914
	6	0.548	3,969	0.344	0.9786
	7	0.563	7,211	0.441	0.9889
Dilative	8	0.599	13,330	0.306	-0.1450
	9	0.626	11,936	0.578	0.1690
	10	0.606	9,141	0.161	0.1094
	11	0.608	12,226	0.485	-7.8139
	12	0.616	12,270	0.547	-7.3210
	13	0.639	11,468	0.289	0.8769
	14	0.785	2,059	0.503	0.9775

• First, model parameters H_u, H_R, k, and α were evaluated in the least-squares sense for 14 cases of experimental data in Park and Santamarina (2020).

• The optimized parameters simulated the long-term response for number of cycles $i > 100$.

• The simulation was stopped when the difference in void ratio between the end of two consecutive depressurizations did not exceed $e_{i+1} - e_i < 10^{-6}$.

• The last computed void ratio was determined as the terminal void ratio e_T with the corresponding number of cycles N_T.

3.4.1 Two-surface plasticity model

Fig. 6 presents the evolution of the void ratio for contractive and dilative sand specimens as a function of the number of pressure cycle i where symbols indicate experimental results from Park and Santamarina (2020) and the lines fitted on data correspond to the modified two-surface plasticity model in this study. Table 4 summarizes the optimized model parameters, the coefficient of determination R^2 for the dataset, and the terminal void ratio e_T evaluated via the abovementioned procedure.

The modified two-surface plasticity model adequately describes the dataset of Park and Santamarina (2020). In general, the coefficient of determination R^2 values for contractive cases is much higher than for dilative cases (i.e., No. 1 ~ 7 for contractive and No. 8 ~ 14 for dilative in Tables 2 and 4). This difference is due to the higher quality of experimental data in contractive sands and the larger variation of the void ratio in dilative sands. Thus, the modified plasticity model determines the terminal void ratio e_T of dense sand specimens for a number of cycles of less than 100. The extremely low variation of volumetric changes for dense sands (cases No. 8 ~ 12) results in the negative R^2 values associated with the small total sum of squares. Additionally, the two surface plasticity model proposed in this study cannot properly capture the terminal void ratio for case No. 2 due to the semi-linear decrease trend in the experimental data. Therefore, the simulation for case No. 2 was terminated when the computed void ratio reached the minimum value (i.e., $e_{min} = 0.522$, see Table 1) after $i = 39{,}005$ cycles.

3.4.2 Hyperbolic model

For comparison, Table 5 lists the terminal void ratio e_T determined by fitting the hyperbolic model using all experimental results (Eq. (20)). The hyperbolic model also adequately describes the observed dataset; however, it leads to lower terminal void ratio e_T for contractive and higher e_T for dilative sand samples (except the case No. 2). In addition, higher R^2 values summarized in Table 5, particularly for dilative samples, indicate that the hyperbolic model better describes the low-quality data. Apart from the simplicity of the model, it may be advantageous to use the hyperbolic model for predicting the terminal void ratio for cases that cannot be well described by the two-surface plasticity model as discussed later in the discussion section.

4. Discussion

4.1 Terminal void ratio

Fig. 7 shows a comparison between the initial void ratio e_o and the terminal void ratio e_T estimated using both the modified two-surface plasticity model and the hyperbolic model with the critical state line *CSL* in p'-e space. The terminal void ratio e_T for all contractive specimens (illustrated with blue) tends to be smaller than the critical state void ratio e_{cs} regardless of the model type while the variations of the void ratio are more significant when using the hyperbolic model except for specimen No. 2. This larger variation of the void ratio in the hyperbolic model than the modified two surface plasticity model is also evaluated for the dilative specimens. In particular, the terminal void ratio for specimen No. 14 in contractive side indicates that the hyperbolic model overestimates the variation of the void ratio for sands when subjected to repetitive changes in pore fluid pressure under drained conditions.

The critical state is one of the examples for the terminal state of soils. The critical state line *CSL* for granular materials is defined under monotonic load and very large strain conditions. When medium-dense sands (case No. 4, 5, and 6) experience repetitive loads under drained conditions, they can be denser than the critical state (Narsilio and Santamarina 2008, Park and Santamarina 2020). However, the two-surface plasticity model fails to capture the terminal void ratio for specimen No. 2 and its void ratio reaches the minimum void ratio. In contrast, the hyperbolic model well tracks the void ratio for specimen No. 2 with a higher R^2 value and the estimated terminal void ratio is close to the *CSL*. Therefore, the hyperbolic model can be used to predict the terminal void ratio for cases where the two-surface plasticity model cannot predict the terminal void ratio due to the scattering of the measured void ratio or a semi-linear dataset.

4.2 Influence of slope α

The slope α for the model constant H_u in Eq. (21)

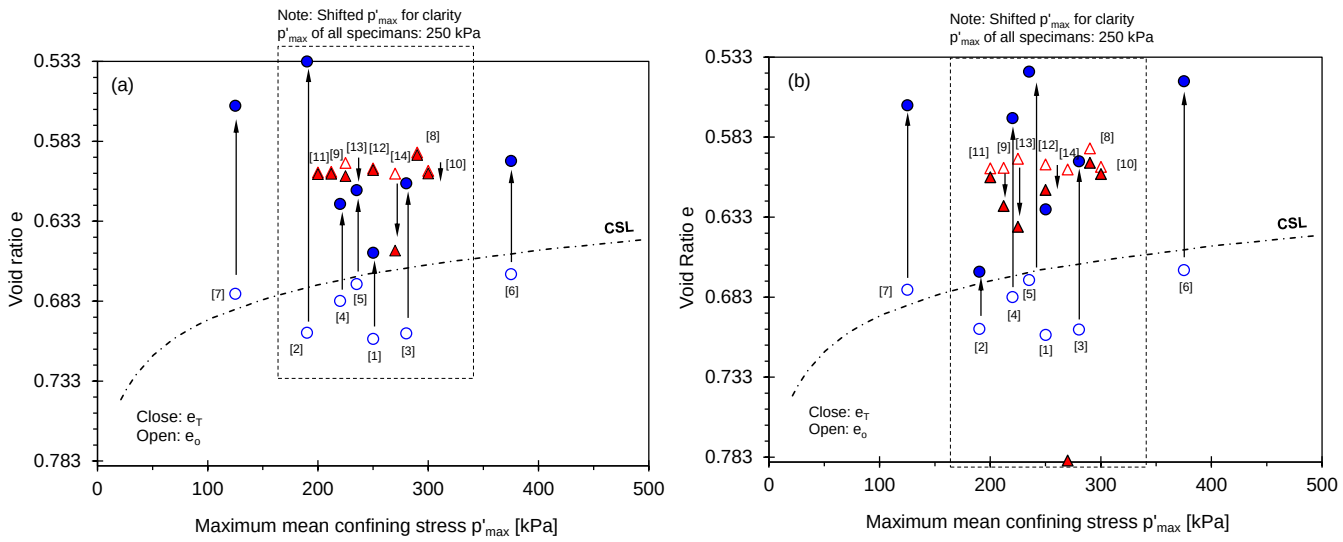

Fig. 7 Comparison between the initial void ratio e_o and the terminal void ratio e_T estimated using (a) the modified two-surface plasticity model and (b) the hyperbolic model

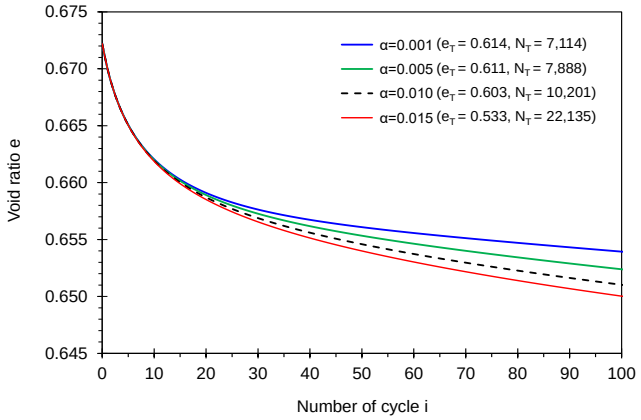

Fig. 8 Void ratio computed from the two-surface plasticity model versus pressure cycle with different slope α values (note: this analysis uses the model parameters for case No. 5 in Table 4)

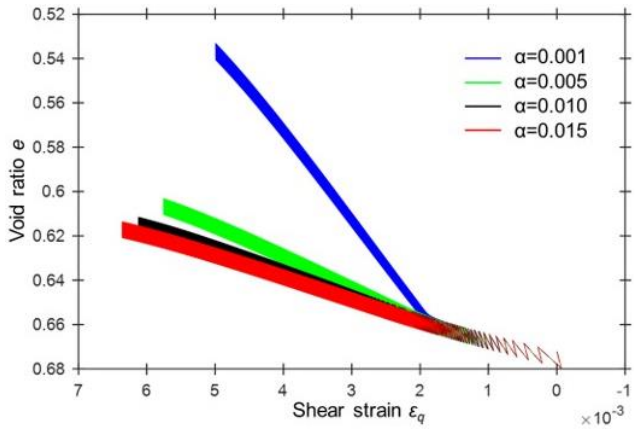

Fig. 9 Change in void ratio e versus shear strain ε_q with different α values for case No. 5 in Table 4 (note: the number of cycles i = 1-to-10^5)

determines the increment rate of plastic moduli H_{unload} and H_{load}, which affects the evolution of the void ratio and the terminal void ratio. Fig. 8 presents the void ratio evolution with increasing number of cycles computed using the two-surface plasticity model for different slope α values. For higher slope values, the change in void ratio becomes larger, which in turn leads to a smaller terminal void ratio e_T and a larger number of cycles N_T required to reach the terminal state. This analysis implies that the estimated terminal void ratio is highly sensitive to the experimental dataset, especially when the dataset is limited and only available until a cycle number less than 100. Therefore, a small variation of the dataset at a low number of cycles (e.g., measurement error) can lead to significant underestimation/overestimation of the terminal void ratio.

In addition, the slope α also affects the shear strain accumulation ε_q of soils as presented in Fig. 9. The change in void ratio plotted against deviatoric strain demonstrates that a higher α value leads to more pronounced shear strain accumulation. This observation indicates that the selection of the slope α value requires special attention and model calibration should be conducted based on experimental data to anticipate the long-term accumulation of volumetric/shear strain in sediments.

4.3 Limitation of the modified two-surface plasticity model

The prediction method for terminal void ratios using the two-surface plasticity model demonstrated in this study has a limitation, particularly for dilative specimens. Since the algorithm used in this work for finding the best curve-fit returns the modeled void ratio values in the least-square sense, the low variation of the observed void ratio in cases No. 8-to-13 causes a decrease in the modeled void ratio for a number of cycles less than 100.

In contrast, the dilative specimen with a high variation of void ratio in case No. 14 can be relatively well described by the proposed model until a number of cycles i < 1000. However, the modeled void ratio also decreases at a large number of cycles i > 1000 for case No. 14, and all modeled

dilative specimens eventually reach the minimum void ratio above 1000 cycles. This decreasing trend of the void ratio of dilative specimens is physically unlikely to take place, and therefore estimating the long-term response of dilative specimens for case No. 14 is unfeasible. The trial-and-error method of parameter modifications listed in Table 4 enabled us to overcome the limitations addressed above; yet, the predicted terminal void ratio of dilative cases remains researcher-dependent. Further investigation or modification is required to eliminate the limitations of the proposed model.

5. Conclusions

This study builds on earlier efforts towards modeling the soil response to repetitive loads combined with experimental data obtained from the literature. We propose a new method to predict the terminal void ratio e_T of soils subjected to repetitive changes in pore-fluid pressure during a large number of pressure cycles under triaxial loading and drained conditions. This method uses the trust-region algorithm to obtain the best-modeled void ratio profile for the given observational data. The modified two-surface plasticity model adopted in this study allows us to anticipate the terminal void ratio e_T for contractive and dilative sands when subjected to cyclic changes in pore water pressure. The slope α in the modified model appears to be critical for the determination of the increment rate of plastic moduli, and the model adequately captures the evolution of the void ratio with increasing number of cycles. The empirical-based hyperbolic model can be used to predict the terminal void ratio in cases where the two-surface plasticity model cannot properly function due to the scattering of measured data or to a semi-linear dataset. The modified bounding surface model presented in this study enables the asymptotic state of soils to be estimated from experimental data for a relatively low number of cycles.

The terminal density estimated in this study represents the potential settlement for sediments subjected to cyclic loads. However, shear response under cyclic loading conditions involves shakedown or ratcheting, which are independent of the volumetric response. Therefore, further development of the validated constitutive model with experimental shear strain data is required to reflect shear stain accumulation under cyclic loadings. The developed model will improve the understanding of the long-term volumetric and shear responses of soil when subjected to repetitive loads.

Acknowledgments

This work was supported by the 2020 Research Fund of the University of Ulsan.

References

Anderson, K.H. (2009), "Bearing capacity under cyclic loading-offshore, along the coast, and on land", *Can. Geotech. J.*, **46**(5), 513-535. https://doi.org/10.1139/T09-003.

Bardet, J.P. (1986), "Bounding surface plasticity model for sands". *J. Eng. Mech.*, **112**(11), 1198-1217. https://doi.org/10.1061/(ASCE)0733-9399(1986)112:11(1198).

Boulon, M. and Foray, P. (1986), "Physical and numerical simulation of lateral shaft friction along offshore piles in sand", *Proceedings of the 3rd International Conference on Numerical Methods in Offshore Piling*, Nantes, France, May.

Chu, J., Leroueil, S. and Leong, W.K. (2003), "Unstable behaviour of sand and its implication for slope instability", *Can. Geotech. J.*, **40**(5), 873-885. https://doi.org/10.1139/t03-039.

Dafalias, Y.F. and Herrmann, L.R. (1982), *A Generalized Bounding Surface Constitutive Model for Clays*, in *Application of Plasticity and Generalized Stress-Strain in Geotechnical Engineering,* American Society of Civil Engineers, 78-95.

Dafalias, Y.F. and Popov, E.P. (1975), "A model of nonlinearly hardening materials for complex loadings", *Acta Mech.*, **21**(3), 173-192. https://doi.org/10.1007/BF01181053.

Gambolati, G. and Teatini, P. (2015), "Geomechanics of subsurface water withdrawal and injection", *Water Resour. Res.*, **51**(6), 3922-3955. https://doi.org/10.1002/2014WR016841.

Hu, C., Liu, H. and Huang, W. (2012), "Anisotropic bounding-surface plasticity model for the cyclic shakedown and degradation of saturated clay", *Comput. Geotech.*, **44**, 34-47. https://doi.org/10.1016/j.compgeo.2012.03.009

Jeong, S., Park, J., Ko, J. and Kim, B. (2017), "Analysis of soil resistance on drilled shafts using proposed cyclic p-y curves in weathered soil", *Geomech. Eng.*, **12**(3), 505-522. http://doi.org/10.12989/gae.2017.12.3.505.

Krieg, R.D. (1975), "A practical two surface plasticity theory", *J. Appl. Mech.*, **42**(3), 641-646. https://doi.org/10.1115/1.3423656.

Leroueil, S., Chu, J. and Wanatowski, D. (2009), "Slope instability due to pore water pressure increase", *Proceedings of the 1st Italian Workshop on Landslides*, Naples, Italy, June.

Manzari, M.T. and Dafalias, Y.F. (1997), "A critical state two-surface plasticity model for sands", *Géotechnique*, **47**(2), 255-272. https://doi.org/10.1680/geot.1997.47.2.255.

Moghaddas Tafreshi, S.N., Darabi, J. and Dawson, A. (2018), "Cyclic loading response of footing on multi-layered rubber-soil mixtures", *Geomech. Eng.*, **14**(2), 115-129. http://doi.org/10.12989/gae.2018.14.2.115.

Molina-Gomez, F., Caicedo, B. and Viana da Fonseca, A. (2019), "Physical modelling of soil liquefaction in a novel micro shaking table", *Geomech. Eng.*, **19**(3), 229-240. http://doi.org/10.12989/gae.2019.19.3.229.

Narsilio, A. and Santamarina, J.C. (2008), "Terminal densities", *Geotechnique,* **58**(8), 669-674. https://doi.org/10.1680/geot.2008.58.8.669.

Niemunis, A. and Herle, I. (1997), "Hypoplastic model for cohesionless soils with elastic strain range", *Mech. Cohesive-Frict. Mater.*, **2**(4), 279-299. https://doi.org/10.1002/(SICI)1099-1484(199710)2:4<279::AID-CFM29>3.0.CO;2-8

Nikitas, G., Arany, L., Aingaran, S., Vimalan, J. and Bhattacharya, S. (2017), "Predicting long term performance of offshore wind turbines using cyclic simple shear apparatus", *Soil Dyn. Earthq. Eng.*, **92**, 678-683. https://doi.org/10.1016/j.soildyn.2016.09.010.

Olson, S.M., Stark, T.D., Walton, W.H. and Castro, G. (2000), "1907 static liquefaction flow failure of the north dike of Wachusett dam", *J. Geotech. Geoenviron. Eng.*, **126**(12), 1184-1193. https://doi.org/10.1061/(ASCE)1090-0241(2000)126:12(1184).

Park, J. (2018), "Long-term response of soils subjected to repetitive mechanical loads: Engineering implications," Ph.D. Dissertation, Georgia Institute of Technology, Atlanta, Georgia, U.S.A.

Park, J. and Santamarina, J.C. (2019), "Sand response to a large number of loading cycles under zero-lateral-strain conditions: evolution of void ratio and small-strain stiffness", *Géotechnique*, **69**(6), 501-513. https://doi.org/10.1680/jgeot.17.P.124.

Park, J. and Santamarina, J.C. (2020), "Soil response to repetitive changes in pore-water pressure under deviatoric loading", *J. Geotech. Geoenviron. Eng.*, **146**(5), 04020023. https://doi.org/10.1061/(ASCE)GT.1943-5606.0002229.

Pasten, C., Shin, H. and Santamarina, J.C. (2014), "Long-term foundation response to repetitive loading", *J. Geotech. Geoenviron. Eng.*, **140**(4), 04013036. https://doi.org/10.1061/(ASCE)GT.1943-5606.0001052.

Peng, J., Clarke, B.G. and Rouainia, M. (2006), "A device to cyclic lateral loaded model piles", *Geotech. Test. J.*, **29**(4), 341-347. https://doi.org/10.1520/GTJ100226.

Pisanò, F. and Jeremić, B. (2014), "Simulating stiffness degradation and damping in soils via a simple visco-elastic–plastic model", *Soil Dyn. Earthq. Eng.*, **63**, 98-109. https://doi.org/10.1016/j.soildyn.2014.02.014.

Sonmezer, Y.B. (2019), "Investigation of the liquefaction potential of fiber-reinforced sand", *Geomech. Eng.*, **18**(5), 503-513. http://doi.org/10.12989/gae.2019.18.5.503.

Suryatriyastuti, M.E., Mroueh, H. and Burlon, S. (2014), "A load transfer approach for studying the cyclic behavior of thermo-active piles", *Comput. Geotech.*, **55**, 378-391. https://doi.org/10.1016/j.compgeo.2013.09.021.

Wu, Y., Hyodo, M. and Aramaki, N. (2018), "Undrained cyclic shear characteristics and crushing behaviour of silica sand", *Geomech. Eng.*, **14**(1), 1-8. http://ddoi.org/10.12989/gae.2018.14.1.001.

Yu, H.S. (1998), "CASM: A unified state parameter model for clay and sand", *Int. J. Numer. Anal. Met.*, **22**(8), 621-653. https://doi.org/10.1002/(SICI)1096-9853(199808)22:8<621::AID-NAG937>3.0.CO;2-8

Yu, H.S. (2007), *Plasticity and Geotechnics*, Springer, New York, U.S.A.

Yu, H.S. and Khong, C.D. (2003), "Bounding surface formulation of a unified critical state model for clay and sand", *Proceedings of the 3rd International Symposium on Deformation Characteristics of Geomaterials, IS Lyon 2003*, Lyon, France, September.

Yu, H.S., Khong, C. and Wang, J. (2007), "A unified plasticity model for cyclic behaviour of clay and sand", *Mech. Res. Commun.*, **34**(2), 97-114. https://doi.org/10.1016/j.mechrescom.2006.06.010.

Zhang, B., Mei, C., Huang, B., Fu, X., Luo, G. and Lv, B. (2017), "Model tests on bearing capacity and accumulated settlement of a single pile in simulated soft rock under axial cyclic loading", *Geomech. Eng.*, **12**(4), 611-626. http://doi.org/10.12989/gae.2017.12.4.611.

GC